Journal of Alloys and Compounds 509 (2011) 4636–4642

Contents lists available at ScienceDirect

Journal of Alloys and Compounds

journal homepage: www.elsevier.com/locate/jallcom

Influence of Mg content on quench sensitivity of Al–Zn–Mg–Cu aluminum alloys

Yun-lai Deng[a,b,*], Li Wan[a,b], Yun-ya Zhang[a,b], Xin-ming Zhang[a,b]

[a] School of Materials Science and Engineering, Central South University, Changsha 410083, China
[b] Key Laboratory of Nonferrous Materials Science and Engineering, Ministry of Education, Changsha 410083, China

ARTICLE INFO

Article history:
Received 28 August 2010
Received in revised form 17 January 2011
Accepted 21 January 2011
Available online 2 February 2011

Keywords:
Al–Zn–Mg–Cu
End-quenching
Quench sensitivity
Microstructure

ABSTRACT

The influence of Mg content on quench sensitivity of Al–8.0Zn–*x*(=1.0–2.0)Mg–1.6Cu alloys was investigated by an end-quenching test method. The depths of age hardening layer referenced to hardness retention values (e.g., 90%) of the end-quenched samples were used to describe the quench sensitivity. The results showed that the depths of age hardening layer decreased with increase of Mg content. The amount of the equilibrium-state $MgZn_2$ (η) particles was the primary factor that determined the depths of age hardening layer. The η particles underwent two precipitation processes successively with decrease of cooling rate during quenching: precipitation on grain boundaries and precipitation inside the grains. The precipitation temperature peaks rose, and the ranges of the temperatures are extended with the increase of Mg content. A preliminary prediction has been made for the initial precipitation temperatures and the temperature peaks satisfying linear relation with Mg content (wt.%).

1. Introduction

Aeronautical and aerospace industries are developing rapidly, and the use of monolithic components could help in reducing component weights significantly as well as lower assembly costs. Accordingly, the fabrication of large monolithic components using 7*xxx* series Al alloys thick plates has attracted increasing attention because they have superior mechanical properties [1–3]. However, because of their relatively high quench sensitivity, there is a significant difference in the mechanical properties from the surface to the center after quenching-aging [4–8]. As a result, Alcoa Company developed the 7050 and 7150 alloys, in which quench sensitivities are lower than those of 7075 alloy, and used them in the Boeing 757, 767, and 777 aircrafts [9,10]. The quench sensitivities of various Al alloys and addition of trace elements (e.g., Cr, Zr) have been reported in many papers [4,11–14]. In 2003, Alcoa Company developed 7085 Al alloy, which has high strength and toughness and low quench sensitivity; this alloy has been used in the advanced aircrafts such as A380 [11]. However, it is well known that when the arithmetic mean of the limit of an Al alloying element in an original alloy is 1.0–2.0 (wt.%), the maximum difference is 0.20 (wt.%). If the component range is exceeded, the Al alloy should be registered as a new Al alloy [15]. In 7085 Al alloy, the Mg content is 1.2–1.8 (wt.%), this accordingly results in more than two types of Al alloys. Therefore, it is important to know the effect of Mg content on quench sensitivity of the 7085-type Al alloys, but few reports have covered this issue.

In present paper, an end-quenching test, which has been used to determine the quench sensitivity of Al alloys and to improve the parameters of water spraying-quench technique [16,17], was employed to identify the effect of Mg content on quench sensitivity of the 7085-type Al alloys. This study will be helpful to develop this type Al alloys.

2. Experimental

The investigated Al–8.0Zn–*x*Mg–1.6Cu alloys were prepared in laboratory by an ingot metallurgical route. The raw materials were high purity Al (99.998%), Zn (99.98%), and Mg (99.98%) and Al–3%Zr, Al–30%Cu, and Al–5%Ti–B (wt.%). The alloys were melted in a graphite crucible heated using an electrical resistance furnace. The liquid metal was then poured into an iron mold to produce 40 mm × 80 mm × 120 mm ingots. The chemical compositions of the alloys are shown in Table 1. The ingots were homogenized at 400 °C for 12 h and then at 470 °C for 12 h. The total thick reduction of rolling deformation was approximately 70%. The initial rolling temperature was 420 °C. Cylinders with dimension of Φ10 mm × 140 mm were cut from the rolled plates as samples used in an end-quenching test. The schematic diagram of the end-quenching test and the water flux and pressure through nozzle used by present paper are shown in Fig. 1. After solution heat treatment at 475 °C for 4 h, the end-quenching tests were conducted, and the end-quenched samples were aged at 121 °C for 24 h. Hardness tests of the aged samples were conducted to obtain the hardness changes along the direction of the distance far from the end-quenched face.

An XJP-6A metalloscope was used to obtain the metallographes, and the corrosive solution was composed of 1 ml HF, 1.5 ml HCl, 2.5 ml HNO_3, and 95 ml distilled water. A JSM-6360LV scanning electron microscopy (SEM) and a TECNAIG^2 20 transmission electron microscopy (TEM) at an acceleration voltage of 200 kV were used to study the second phases. Furthermore, A Rigaku D/Max 2500 diffractometer was used for the X-ray diffraction (XRD) tests. A NET2SCH-200 F3 thermal analyzer was used for differential scanning calorimetry (DSC), with a temperature reduction rate

* Corresponding author at: School of Materials Science and Engineering, Central South University, Yuelu Section, Changsha, Hunan 410083, China.
Fax: +86 731 88876913.
E-mail address: dengylcsu@126.com (Y.-l. Deng).

0925-8388/$ – see front matter © 2011 Elsevier B.V. All rights reserved.
doi:10.1016/j.jallcom.2011.01.147

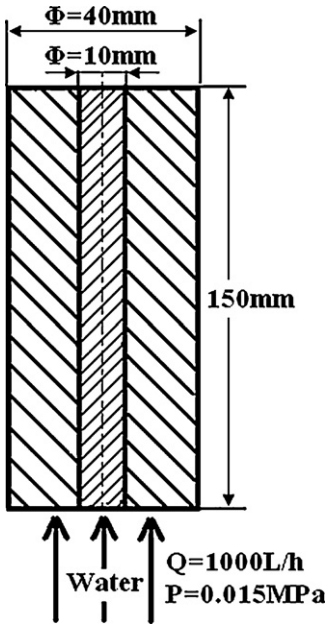

Fig. 1. Schematic diagram of the end-quenching test.

of 5 °C/min from 450 °C. An HV-5 tester was used to measure Vickers hardness (HV) under a load of 3 kg and a hold time of 15 s.

3. Results and analyses

3.1. Hardness curves

The hardness curves of the end-quenching-aging specimens of the 1#, 2#, 3# Al alloys in Table 1 are shown in Fig. 2. It can be seen in Fig. 2(a) that when Mg = 1.0% (1# alloy), HV_{max} = 167, when Mg = 1.4% (2# alloy), HV_{max} = 173, and when Mg = 2.0% (3# alloy), HV_{max} = 197. The reason is that the dominant strengthening particles in the present Al–Zn–Mg–Cu alloys are non-equilibrium η' phase particles, and the increased addition of Mg causes the amount of η' phase particles in the matrix to increase. However, the higher Mg content, the greater decrease of hardness along the direction of the distance far from the end-quenched face (d). This means that the quench sensitivity is influenced by the Mg content in present Al alloys, i.e., the higher Mg content, the more sensitive.

In order to quantitatively describe effect of Mg content on quench sensitivity, the curves of hardness retention value vs d are shown in Fig. 2(b). As mentioned above, the hardness retention value decreases with increase of the d. It is very interesting that the quench sensitivity could be simply described by the depth of age hardening layer, which is evaluated by the distance at where a certain hardness retention value is selected. Here, the selected hardness retention value is 90%, and then for Mg = 1.0, the entirely tested-distance of the specimen can achieve full hardening, and the depth of age hardening layer is more than 100 mm; when Mg = 1.4, the depth of age hardening layer is about 65 mm; when Mg = 2.0, the depth of age hardening layer decreases to about 40 mm. It is also worthy to notice that the deviation distances of the hardness retention values between the specimens of the three alloys become small with the increase of Mg addition, i.e., the deviation occurs at 50 mm between 1# and 2# alloys, whereas 3# alloy almost deviate from 1# and 2# alloys at the beginning. In short, the depths of age hardening layer of the alloys are very sensitive to Mg content.

Table 1
Nominal chemical composition of the investigated Al–Zn–Mg–Cu alloy (wt.%).

Alloy	Zn	Mg	Cu	Zr	Fe	Si	Cr	Mn	Ti	Al
1#	8.0	1.0	1.6	0.13	0.07	0.05	0.03	0.04	0.06	Bal.
2#	8.0	1.4	1.6	0.13	0.07	0.05	0.03	0.04	0.06	Bal.
3#	8.0	2.0	1.6	0.13	0.07	0.05	0.03	0.04	0.06	Bal.

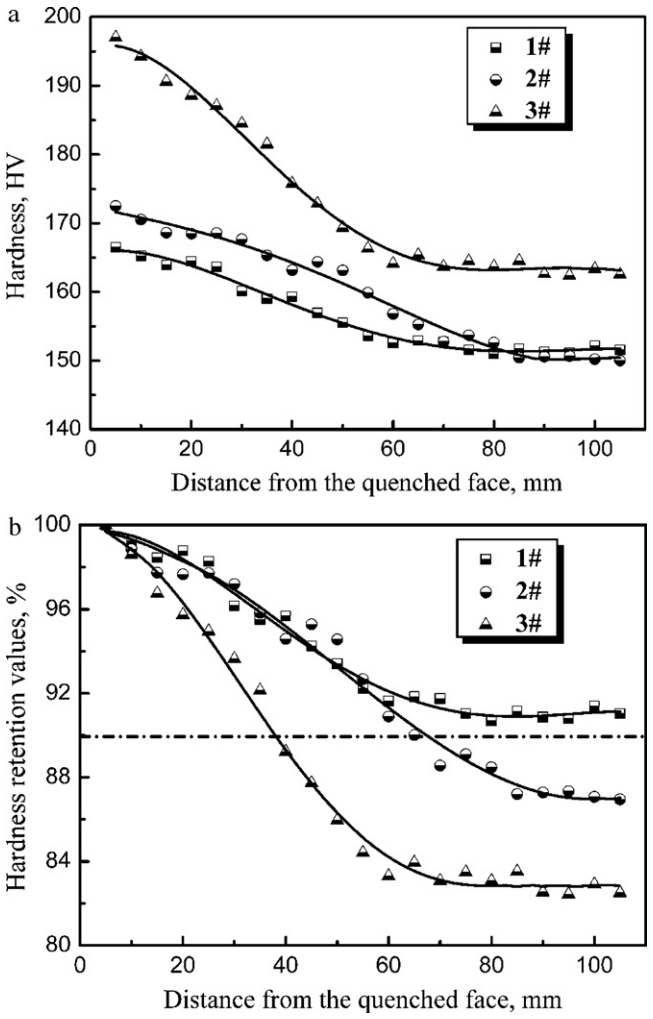

Fig. 2. Aging hardness and hardness retention values curves of the end-quenched samples.

3.2. Microstructures

Stereo metallographic images along the direction with the increasing d in the end-quenched sample of 3# alloy are shown in Fig. 3. It can be seen in Fig. 3(a) that no significant recrystallization occurred during solution heat treatment. The matrix microstructures in the specimen cut from $d \approx 5$ mm of the end-quenched sample still maintains the stripe-shaped grains extended along rolling direction. As the cooling rate of the quenching decreased with the increasing d of the end-quenched sample, significant recrystallization and non-recrystallization areas can be observed in the metallographic images of the specimens cut from $d \approx 40$ mm to $d \approx 80$ mm, respectively, as shown in Fig. 3(b) and (c), respectively. The bright areas are the recrystallization areas, and the dim areas represent the sub-grain structures with precipitations on the sub-grain boundaries.

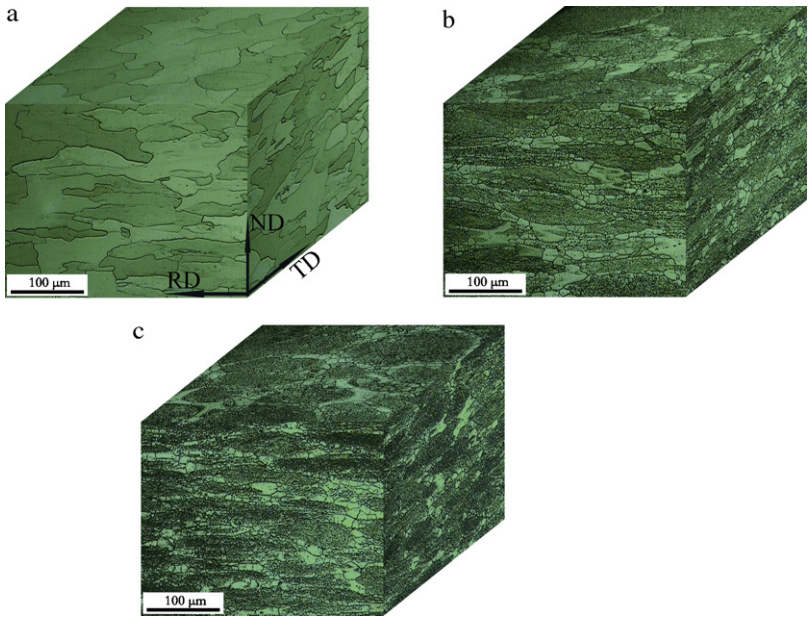

Fig. 3. Optical micrographs of the end-quenched sample of 3# alloy at different distances far from the end-quenched face: (a) 5 mm; (b) 40 mm; (c) 80 mm.

The precipitated particles in the specimens of the $d \approx 5$ mm, 40 mm, and 80 mm cut from the end-quenched sample of 3# alloy have been studied by TEM, the TEM images are shown in Fig. 4. It can be seen in Fig. 4(a) that the strengthening particles inside the grains are mainly η' particles, these particles are small and dispersed as the expected. With increasing distance to 40 mm, the particles become somewhat coarsened, as shown in Fig. 4(b). When $d \approx 80$ mm, some stick-shaped equilibrium-state η particles appear as shown in Fig. 4(c). The coarse precipitated particles on the boundaries in various distances specimens are shown in Fig. 4(d) and (e). It can be seen in Fig. 4(d) that the equilibrium-state η particles on the grain boundaries are discontinuous in the specimen of $d \approx 5$ mm. The image in Fig. 4(e) is typical microstructures of the boundaries in the specimens of $d \approx 40$ mm and 80 mm, a lot of the equilibrium-state η particles precipitating on the grain boundaries are larger than that of $d \approx 5$ mm. When $d \approx 80$ mm, the equilibrium-state η coarse particles precipitate inside the grains, even a considerable number of coarse η particles appear on Al_3Zr particles because of the core of heterogeneous nucleation (Fig. 4(f)). It is obvious that the amount of the equilibrium-state η particles increase because of the cooling rate being slower with the increase of the d in the end-quenched specimens. It is no doubt that the η particles causes the amount of strengthening η' particles to decrease. Therefore, the hardness decreases with the increase of the d (Fig. 2(a)).

The increased addition of Mg causes a large increase of the supersaturation solubility in the matrix before quenching, so the driving force of η precipitations increases during quench, and then the decrease of hardness, i.e., the retention hardness value, of 3# alloy with the maximum Mg content is the most significant.

3.3. Behaviors of the precipitations

The differential scanning calorimetry (DSC) cooling analyses were conducted at a cooling rate of 5 °C/min. The DSC curves of the specimens cut from 1#, 2#, and 3# alloys are shown in Fig. 5. It can be seen that each of the three alloys exhibited two superimposed exothermic effect, and the exothermic effects become more significant with the increase of Mg content. The statistics for the temperatures of the DSC curves in Fig. 5 are listed in Table 2. It can be seen that the temperatures at which the effect appear and the effect peaks advance substantially with the increased addition of Mg. The temperatures at which the effects stopped were consistent, i.e., about 218 °C.

The microstructures of the 3# alloy specimens were observed after heat insulation were performed for the corresponding exothermic effects. Fig. 6 shows the metallographic images in the ND–RD section. It can be seen in Fig. 6(a) that the grains have been elongated along the rolling direction. The quenched specimen exhibits fine grain boundaries with clean grains inside, indicating that the second-phase particles in the solution heat treatment have been dissolved into the matrix and formed a supersaturated sosoloid. No significant precipitation particles occurred during the quenching process. After heat insulation at 405 °C for 1 h, as shown in Fig. 6(b), the microstructures inside the grains still cleanly remained; however, there is significantly discontinuous precipitation of the second-phase particles at the boundaries. After heat insulation at 340 °C for 1 h Fig. 6(c), there are not only obvious the discontinuous second-phase particles on the boundaries but the microstructures inside the grains are no longer clean; many precipitations occurred.

Fig. 7 shows the corresponding SEM images of the rolling plane to the quenched specimen. Nearly all the second-phase particles in the quenched specimen, as shown in Fig. 7(a), is in accordance with the metallographic image Fig. 6(a). There is a small number of 1–2 μm white particles in the matrix. Semi-quantitative analyses by energy disperse spectroscopy (EDS) show that these white particles are in the Fe-rich phases. Owing to their small number, these particles probably absorb the matrix signals dur-

Table 2
Statistical temperatures for heat effect peaks (determined by tangent method).

Alloy	A (°C)	B (°C)	C (°C)	D (°C)	A–D (°C)
1#	359 ± 3	328 ± 2	283 ± 2	218 ± 2	141 ± 5
2#	403 ± 3	357 ± 3	326 ± 2	220 ± 5	183 ± 8
3#	438 ± 2	387 ± 2	342 ± 2	215 ± 3	223 ± 5

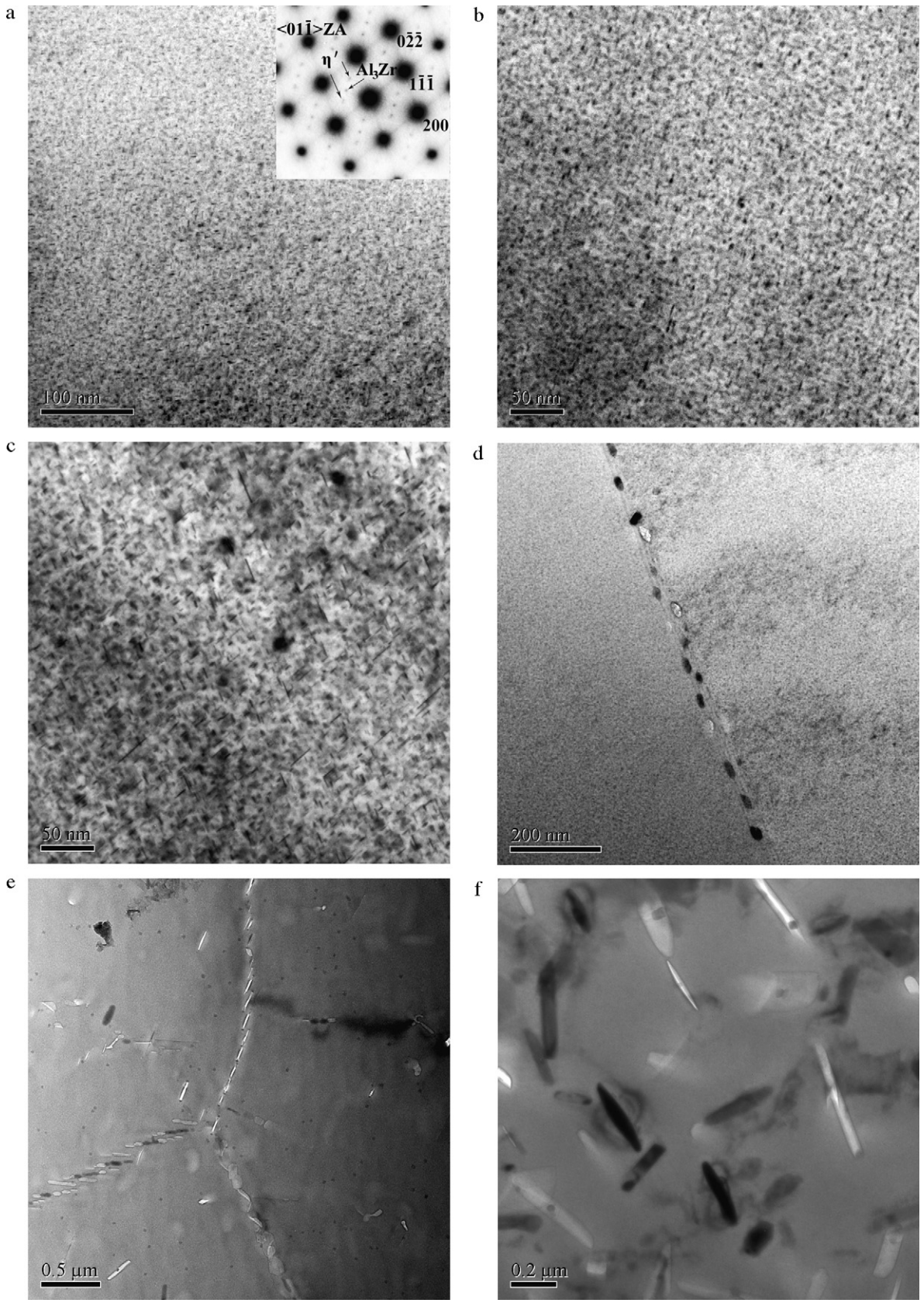

Fig. 4. Typical TEM microstructures of the end-quenched sample of 3# alloy at different distances far from the end-quenched face: (a) 5 mm; (b) 40 mm; (c) 80 mm.

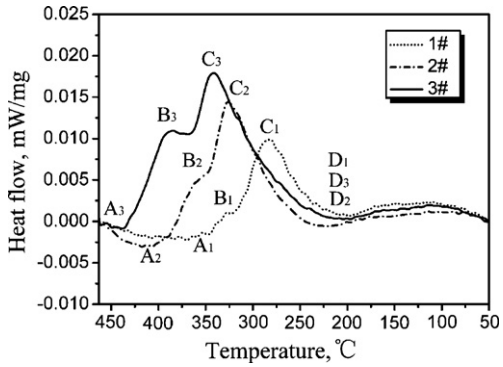

Fig. 5. DSC curves of the specimens of 1#, 2#, and 3# alloys during the cooling process.

ing the EDS computation, and their stoichiometric ratios approach those of Al_7Cu_2Fe phase. For fabrication of this type alloys, the number and size of Fe-rich particles should be strictly controlled. Because of their stable properties, it is generally believed that they could not be dissolved completely in either the homogenization or the solution heat treatment and that their eventual dissolution would definitely be followed by matrix fusion. These particles would, therefore, significantly affect the mechanical properties of the alloys. The microstructures in Fig. 7(b) after heat insulation at 405 °C for 1 h show that the second-phase particles significantly precipitate on grain and sub-grain boundaries. However, few η particles precipitate inside the grains, even inside the recrystallized grains containing incoherent Al_3Zr particles, which could provide heterogeneous nucleation mechanism of the precipitation in the 7085-type Al alloys. The microstructures after heat insulation at 340 °C for 1 h in Fig. 7(c) show a large amount of phase particles have precipitated on the boundaries, and many second-phase particles have precipitated inside the recrystallized grains and subgrains. The EDS analyses show that they are probably also η phase. The activation energy for the precipitation of η phase particles on the boundaries during the quenching process is therefore lower than that inside grains, and the precipitations are consistent with that shown in the metallographic images in Fig. 6(c).

Fig. 8 shows the XRD diffraction results. Compared with the SEM images (Fig. 7(a)) of the quenching state, it can be seen that the Al_7Cu_2Fe phase in the quenched specimen (notation A in Fig. 8) is not detected by XRD because of small amount. After heat insulation at 405 °C for 1 h, there are η phase appears in the matrix (notation B in Fig. 8); η-phase is also determined in the matrix after treatment at 340 °C for 1 h (notation C in Fig. 8). Furthermore, the value of diffraction intensity is found to be higher in the latter case. It is suggested that more η-phase particles have precipitated from the matrix in this state; this agrees with the observations in Figs. 6 and 7.

Statistical analysis of the precipitation temperature ranges and temperature peaks, according to the general tangential method, for the second-phase particles are shown in Table 2. It can be seen from Fig. 9 that all the temperatures approximately satisfy linear relation with Mg content in the alloys, and the influence of Mg addition on initial precipitation temperature and the temperature peak can be clearly seen. This would be helpful to produce this type of alloys.

As mentioned above, it can be concluded that the distributions, quantities, and dimensions of the precipitated particles during end-quenching process are affected by both the addition of Mg content and the distance far from the end-quenched face. The same sample dimensions and water spraying parameters (pressure and flux) used by every end-quenched sample in this paper should make almost the same cooling rate at the same distance; this makes it easy to focus on the quench sensitivity via the depth of age hardening layer according to the hardness retention value (e.g., 90%). It is found that the depths of age hardening layer are sensitive to the Mg content in the 7085-type alloys. It is obvious that the end-quenching test is quicker than general *C*-curves method as expected. Those specimens cut from different distance from the end-quenched samples have different microstructures and hardness values, this is consistent with a basic rule of Al alloys, i.e., the slower cooling rate during quenching, the poorer mechanical properties with more amount of equilibrium-state η-phase particles after aging.

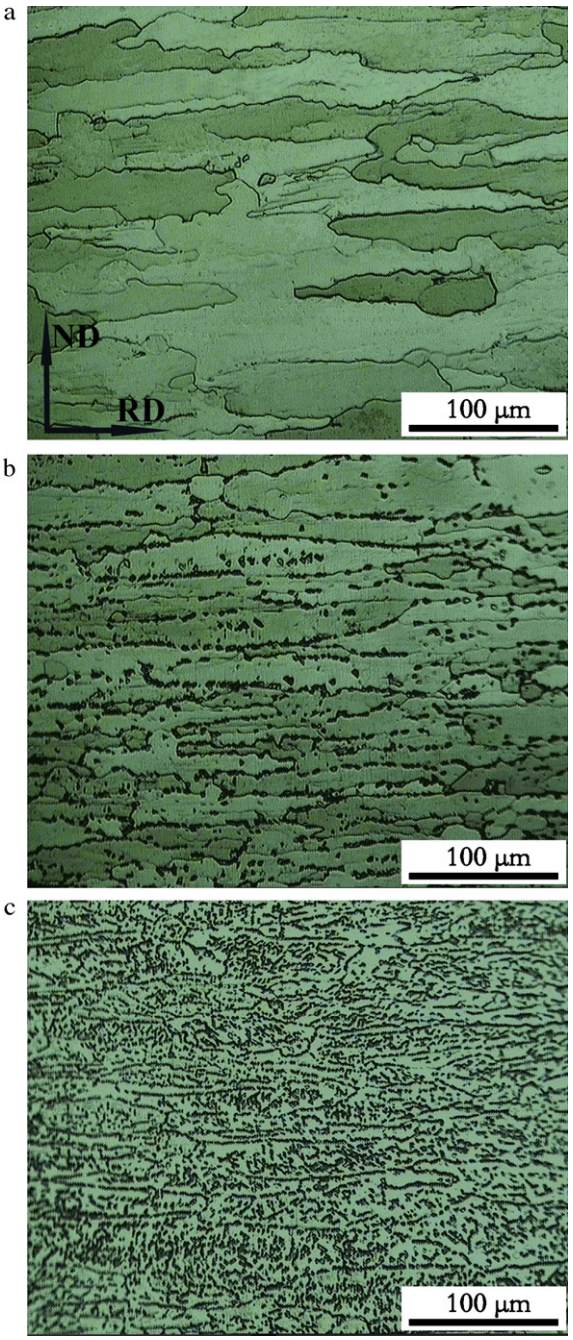

Fig. 6. Optical micrographs of specimens of 3# alloy at: (a) quenching temperature; (b) 405 °C/1 h; (c) 340 °C/1 h.

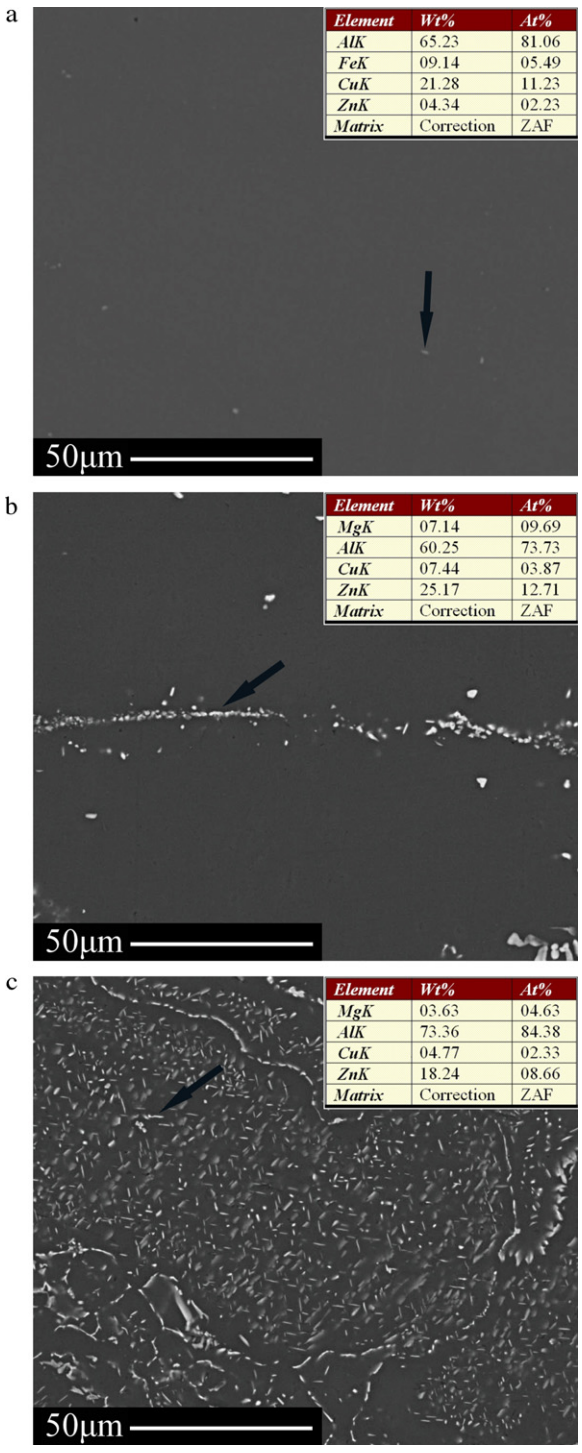

Fig. 7. Typical microstructure of backscattered electron images of the specimens of 3# alloy at: (a) quenching temperature; (b) 405 °C/1 h; (c) 340 °C/1 h.

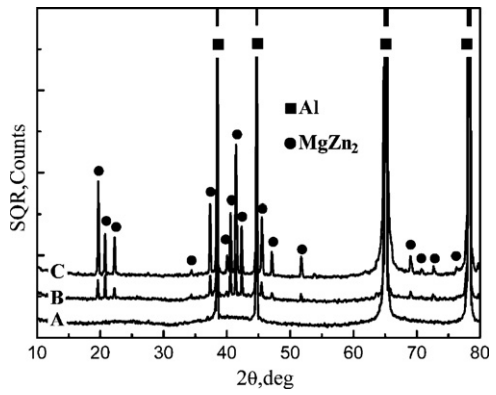

Fig. 8. XRD analysis of specimens of 3# alloys at: (a) quenching temperature; (b) 405 °C/1 h; (c) 340 °C/1 h.

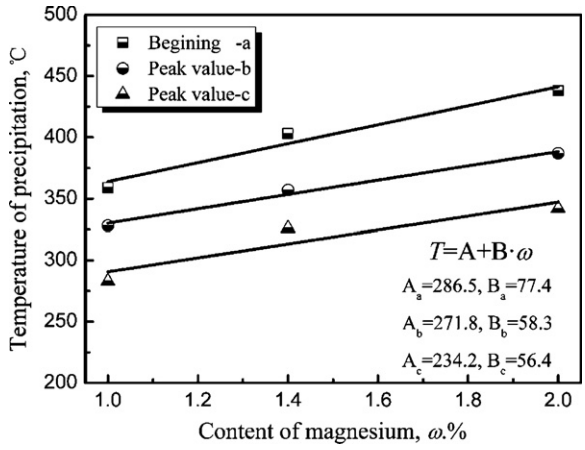

Fig. 9. Relationships between the corresponding temperatures and Mg content (wt.%).

4. Conclusions

(1) An end-quenching test method in this paper makes it easy to investigate quench sensitivity of Al alloys via depth of age hardening layer according to hardness retention value (e.g., 90%). It is obvious that the end-quenching test is quicker than general *C*-curves method.
(2) It is found that the maximum hardness values of these 7085-type (Al–8.0Zn–(1.0–2.0) Mg–1.6Cu) alloys increases with increase of Mg content. However, the depths of age hardening layer decrease significantly too.
(3) It is again verified that the precipitation of the equilibrium-state η particles is the primary factor that determined the depths of age hardening layer of this type Al alloys. The η particles undergo two precipitation processes successively with decrease of cooling rates or increase of distance from the quenched face: nucleation precipitation at boundaries and precipitation inside grains.
(4) As Mg content increased, the driving force of η precipitation increases, and the precipitation temperature peaks rises, and the ranges of the temperatures are extended.
(5) A preliminary prediction could be made for the initial precipitation temperatures and the temperature peaks satisfying linear relation with Mg content (wt.%) in these 7085-type alloys, This should be helpful to production of this type alloys.

Acknowledgement

The authors gratefully acknowledge the financial support by the National Basic Program of China (no. 2005CB623700 and 2010CB731700).

References

[1] A. Heinza, A. Haszler, C. Keidel, S. Moldenhauer, R. Benedictus, W.S. Miller, Mater. Sci. Eng. A 280 (2000) 102.
[2] I.N. Fridlyander, Mater. Sci. Forum 331–337 (2000) 921.
[3] J.C. Williams, E.A. Starke, Acta Mater. 51 (2003) 5775.
[4] M. Conserva, P. Fiorini, Metall. Mater. Trans. B 4 (1973) 857.

[5] D.S. Thompson, B.S. Subramanya, S.A. Levy, Metall. Mater. Trans. B 2 (1971) 1149.
[6] J.S. Robinson, R.L. Cudd, D.A. Tanner, G.P. Dolan, J. Mater. Process. Technol. 119 (2001) 261.
[7] S.D. Liu, X.M. Zhang, M.A. Chen, J.H. You, Mater. Char. 59 (2008) 53.
[8] D. Godard, P. Archambault, E. Aeby-Gautier, G. Lapasset, Acta Mater. 50 (2002) 2319.
[9] T.S. Srivatsan, Int. J. Fatigue 13 (1991) 313.
[10] B. Smith, Adv. Mater. Process. 9 (2003) 41.
[11] D.J. Chakrabarti, J. Liu, R.R. Sawtell, G.B. Venema, Mater. Forum 28 (2004) 969.
[12] M. Conserva, E. Di Russo, O. Caloni, Metall. Mater. Trans. B 2 (1971) 1227.
[13] S.D. Liu, Q.M. Zhong, Y. Zhang, W.J. Liu, X.M. Zhang, Y.L. Deng, Mater. Des. 31 (2010) 3116.
[14] J. Liu, Mater. Sci. Forum. 519–512 (2006) 1233.
[15] International Alloy Designations and Chemical Composition Limits for Wrought Aluminum and Wrought Aluminum Alloys, The Aluminum Association, Inc., 2009, February.
[16] X.M. Zhang, Y.L. Deng, Y. Zhang. Chin Pat, 200710034410.8, 2007.
[17] X.M. Zhang, Y.L. Deng, L. Wan. Chin Pat, 200920063828.6, 2009.